Introducing Phase Analysis Light Scattering for Dielectric Characterization: Measurement of Traveling-Wave Pumping

Jan Gimsa, Peter Eppmann, and Bernhard Prüger
Institute of Biology, Humboldt University, Berlin, Germany

ABSTRACT Phase analysis light scattering (PALS) was applied to characterize a high-frequency traveling-wave (TW) micropump. Field strength and frequency characteristics were measured for aqueous solutions up to 40 MHz and conductivities of 16 mS/m. The TW field was generated by an ultramicroelectrode array of intercastellated electrodes, which were driven by square-topped signals. Pumping exhibited one major relaxation peak, which strongly increased for conductivities above 4 mS/m. The conductivity dependence of the peak frequency showed an unexpected nonlinear behavior. Around 20 MHz an additional peak caused by electronic resonance was found. Additional coils or capacitors shifted the resonance peak and allowed us to determine the electronic properties of the array. Analysis of distortions in the pump spectra caused by the harmonic content of the driving signals showed that the pump direction is determined by the traveling direction of the field. For measurement of AC-field-induced particle translations, the advantage of PALS over the commonly used microscopic analysis is that it offers an objective method for statistically significant, computerized registration of extremely slow motions. Thus, for dielectric characterization, low field strengths can be used, which is advantageous not only for analyzing liquid pumping, but also for measuring particle translations induced by dielectrophoresis or TW dielectrophoresis.

INTRODUCTION

The dielectric properties of suspended particles or liquid media can be measured by conventional impedance spectroscopy. Alternatively, the frequency dependence of forces induced by AC fields can be analyzed. The forces arise from the interaction of induced charges with the field. Such charges can be induced at particle-suspension medium interfaces or in media with inhomogeneous dielectric properties. In liquids, such inhomogeneities can be the interface of nonmixing media (Melcher and Taylor, 1969) or can be generated by a stable temperature gradient (Müller et al., 1993).

When AC-field induced kinetic phenomena are investigated on single particles, depending on the field quality, translation (dielectrophoresis) or rotation (electrorotation) can be induced. In dielectrophoresis, particles in an inhomogeneous AC field move toward or away from regions of high field strength, depending on their polarizability relative to that of the suspension medium. Dielectric dispersions mediate frequency-dependent changes in the dielectrophoretic force.

In electrorotation, a rotating field induces a dipole moment on the particles. The dipole rotates at the field angular frequency. Any dispersion process causes a spatial phase shift between the rotating external field and the induced dipole moment. The interaction of dipole moment and external field induces a torque, causing individual particle rotation. The torque and, therefore, particle rotation are maximized if the relaxation time of the dispersion process and the period of the external field match. Thus the frequencies of electrorotation peaks correspond to the characteristic frequencies of certain dispersion processes.

Similarly, in a TW field there are certain propagation velocities of the field at which the induced charges exhibit a phase lag. As a result, forces may act on particles or on the fluid interfaces, causing TW dielectrophoresis of particles (Hagedorn et al., 1992; Wang et al., 1994) or TW pumping of liquids (Melcher, 1966; Melcher and Firebaugh, 1967; Müller et al., 1993). Depending on the dispersion process causing the phase lag, pumping may be induced in or against the propagation direction of the field.

Microscopic measurements of particle or medium kinetics are tedious and are restricted to the microscopically accessible particle range. Large numbers of measurements of single particles are required for statistical significance. To overcome these drawbacks, turbidity methods can be applied (Talary and Pethig, 1994). For electrorotation of particles we introduced electrorotational light scattering (ERLS) (Gimsa et al., 1995). It allows the simultaneous registration of the individual movement of many particles within a population and proved the general advantage of dynamic light scattering (DLS) methods for dielectric particle characterization. For ERLS a homodyne DLS setup was used (Eppmann et al., 1996; Prüger et al., 1997). For the measurement of particle translations induced by dielectrophoresis or TW dielectrophoresis, light scattering methods should also be advantageous. Kaler et al. (1988) were not very successful in extracting dielectrophoretic particle spectra by a homodyne setup. Particle translations are commonly analyzed by heterodyne single or dual-beam laser-Doppler setups (Berne and Pecora, 1976; Schätzel, 1987). We believe that dual-beam laser-Doppler setups are most appropriate for dielectrophoretic measurements, because

Received for publication 23 May 1997 and in final form 22 August 1997.
Address reprint requests to Dr. Jan Gimsa, Institut für Biologie, Humboldt-Universität zu Berlin, Invalidenstrasse 42, D-10115 Berlin, Germany. Tel.: +49-30/20-93-84-94; Fax: +49-30/20-93-85-20; E-mail: jan=gimsa@rz.hu-berlin.de.

0006-3495/97/12/3309/08 $2.00

their measuring volume is restricted to the crossing region of the two beams and can therefore be adjusted to an area of known field or medium flow distribution. In contrast to ERLS, no optical anisotropy of the particles is required to allow detection of the field-induced particle movement.

Analysis of the frequency dependence of field-induced movements yields information on the inherent dielectric structure of particles or media. For this, appropriate dielectric models must be found (Fuhr et al., 1985; Sauer and Schlögl, 1985; Paul and Otwinowski, 1991; Hagedorn et al., 1992; Wang et al., 1994; Jones, 1995). Of course, AC field-induced movements of single particles or media can not only be applied to characterization but also to particle and cell manipulation or pumping of fluids (Schnelle et al., 1993). Recently Fuhr et al. (1992) presented a TW-driven micropump. The authors characterized its pumping behavior by microscopic observation of test particles. In this paper we reexamine the pump within a widened frequency and conductivity range, and demonstrate the general advantage of phase analysis light scattering (PALS) for the measurement of AC field-induced medium or particle translations.

PHASE ANALYSIS LIGHT SCATTERING

Classical laser Doppler anemometry (LDA) measures particle translation relative to the static interference fringe pattern in the crossing region of two laser beams that form an ellipsoidal measuring volume. Because the beams possess a Gaussian intensity distribution, the intensity distribution within the measuring volume is also Gaussian. The spacing between the fringes, s, is given by

$$s = \frac{\lambda}{2n \sin(\vartheta/2)} \tag{1}$$

with n, λ, and ϑ standing for the refractive index of the solution, the laser wavelength, and the intersection angle of the two beams, respectively. If a particle traverses the interference region, the scattered light intensity varies sinusoidally, generating a Doppler signal known as "Doppler burst." The velocity of the particle determines the Doppler signal frequency and is usually obtained by spectrum analysis.

The major disadvantage of LDA is that the detectable particle displacement is limited. The smaller the particle velocity, the longer becomes the measuring time required for unambiguous registration of the Doppler frequency. This restriction is overcome by PALS, which uses two laser beams with a small optical frequency difference, ω_s (Miller et al., 1991). This creates an interference region with a moving fringe pattern and allows phase demodulation of the Doppler signal when ω_s is used as a reference. A particle at fixed position in the interference region will scatter light with an intensity varying with frequency ω_s and with an arbitrary but fixed phase shift φ_s relative to the reference signal. No minimum particle velocity is required, because any particle translation causes a time-dependent phase change $\varphi(t)$ of the scattered light signal, with

$$\varphi(t) = \varphi_s + \vec{q}[\vec{x}(t) - \vec{x}(0)] \tag{2}$$

where $\vec{x}(t)$ is the position of the particle and $\vec{q}$ is the scattering vector, its magnitude is given by $q = |\vec{q}| = 4\pi n \sin(\vartheta/2)$. A phase change φ of 2π, or 360°, corresponds to a particle displacement by the fringe spacing s. Hence the phase change directly yields the velocity component of the particle motion perpendicular to the interference fringe pattern. Because q depends only on the crossing angle of the beams but not on the angle or direction of detection, only an incoherent detection setup is required.

If one considers multiparticle scattering from a particle suspension, these relations do not remain that simple. Coherent addition of the light scattered from different particles in the interference region may even result in vanishing signal amplitudes due to destructive interference effects. This may give rise to arbitrarily large phase changes. Therefore, in practice, the average particle velocity is deduced by amplitude weighting of the phase changes. Weighting yields the amplitude-weighted phase difference (AWPD) $Q(\tau)$, which is also known as tangential phase change:

$$Q(\tau) = \int_0^\tau A(t)\phi'(t)\mathrm{d}t \tag{3}$$

Like the phase differences in single particle scattering, $Q(\tau)$ is directly related to the average particle velocity (Schätzel and Merz, 1984; Schätzel, 1987).

MATERIALS AND METHODS

PALS setup

The optical setup is given in Fig. 1 *A*. All optical components of Fig. 1 *A* (Melles Griot GmbH, Darmstadt, Germany) were arranged on an optical bench. A 5 mW HeNe laser (λ = 632.8 nm; Melles Griot) was used. After a beamsplitter, the two Bragg cells in the beam paths introduce a difference of 2.65 kHz into the optical frequencies of both first-order beams. Their crossing region determines the measuring volume. In our setup the effective scattering volume can be approximated from the beam diameter and crossing angle to be ~1 mm^3. For measurements it was focused in the center of the channel to reject reflections from the channel walls. For adjustment, the channel was filled with marker-free solution and the scattering signal minimized. The measuring volume was located outside the microstructure to detect solely the medium pump flow and to discriminate directly induced particle movements (see Müller et al., 1993). During measurements, a stereomicroscope (Stemi100; Carl Zeiss GmbH, Oberkochen, Germany) enabled us to check the chamber for undesired flows or bubbles.

The electronic components are depicted in Fig. 1 *B*. The scattered light was detected through a receiving optic and fed to a photon multiplier (PM) (model H5773-01; Hamamatsu Photonics Deutschland GmbH, Herrsching, Germany) through an optical fiber. The PM signal was fed into a lock-in amplifier (model SR850 DSP; Stanford Research Systems, Sunnyvale, CA). The reference signal was obtained by mixing the two driving signals of the Bragg cells (Bragg cells and driving unit; Laser Components GmbH, Olching, Germany; home-made mixer). Field frequencies and amplitudes of a measuring protocol could be programmed by a personal computer, which also drove the field generator (pulse generator HP8130A; Hewlett

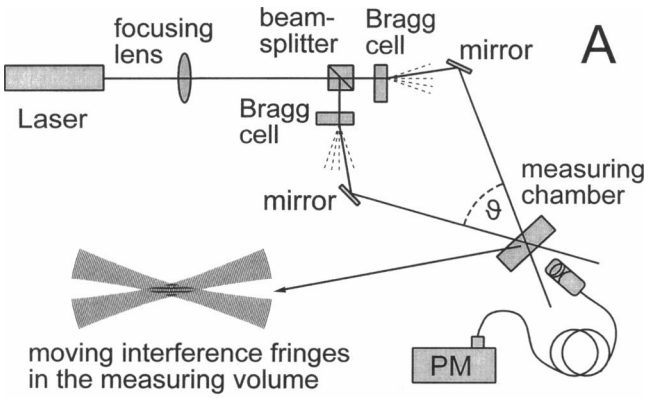

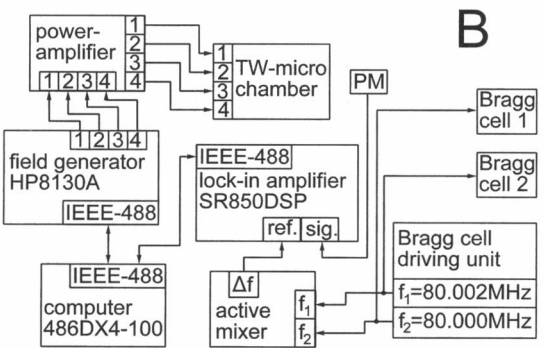

FIGURE 1 Experimental setup for PALS measurements. (*A*) Scheme of the optical setup. The measuring chamber was illuminated by two laser beams 100 μm in diameter. The scattered light intensity was detected by a photomultiplier (PM) through an optical fiber. (*B*) Scheme of the electronic setup. A computer drove the lock-in amplifier and the four phase-field generator.

Packard GmbH, Böblingen, Germany) via an IEEE-488 bus. The four output signals of the generator had a frequency-independent phase shift of 90°. A home-made, four-channel power amplifier allowed us to drive the electrodes with symmetrical square wave signals up to a frequency of 50 MHz and a maximum amplitude of 25 V_{pp}.

Measuring chamber

For measurements of liquid pumping, an optically transparent chamber was used (Fig. 2). The pumping device consisted of a chip with gold electrodes on a quartz-glass wafer. It was mounted on a standard semiconductor ceramic carrier and connected by wire bonding. The planar surface of the electrode array was covered by a glass plate in which a channel with a rectangular cross section was cut. Its length, depth, and width were 4 mm, 100 μm, and 600 μm, respectively. The four 90° phase-shifted signals were applied to 14 electrodes, inducing a TW field in the microchannel. The distance of two neighboring electrodes was 70 μm. Details of chamber fabrication and design were described by Fuhr et al. (1994). To block DC current effects from the electrode structure, the driving signals were capacitively coupled to the microchamber (compare Fig. 7). When the frequency dependence of pumping was measured for different conductivities, no frequencies below 10 kHz were used, to avoid electrode effects and electrolytic degradation of the microstructure.

Measuring solutions

The solution conductivity was adjusted by the addition of KCl to distilled water. For detection of liquid flow by PALS, standard Dow latices (815-nm mean diameter, product no. 44455; Serva, Heidelberg, Germany) were suspended at a low concentration as scattering markers. The suspension was injected into the measuring chamber by a syringe via tubes. The conductivity of the solutions was checked after every measurement. All measurements were carried out at a room temperature of 23°C.

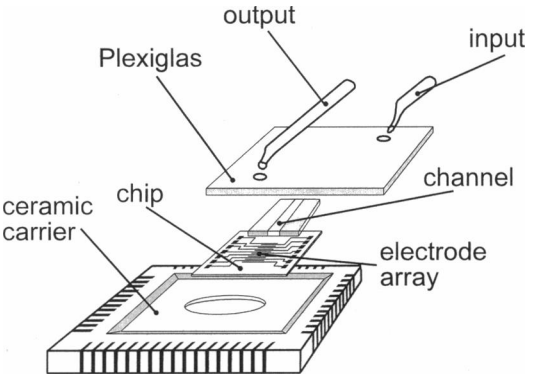

FIGURE 2 Exploded scheme of the TW micropump.

PALS measurements

PALS frequency spectra were measured over more than three decades of the external field frequency. The measuring protocol programmed allowed measurement of complete PALS spectra of 14 field-frequency points within 180 s. Usually, at every field frequency phase and amplitude, values were sampled for 1 s at a sampling rate of 512 Hz and stored to the computer. After measurements the AWPDs were calculated with a simple TurboPascal program. In our setup, pumping in the direction of the TW field yielded negative AWPDs.

RESULTS

Dependence of pumping speed on driving voltage

Fig. 3 presents amplitude-weighted phases (AWPs) and AWPDs of experiments on aqueous pumping. Fig. 3 *A* presents the AWPs for various driving voltages. At every voltage, five data sets, each consisting of 1536 values, are presented. The points of Fig. 3 *B* are means and standard deviations of the AWPDs obtained by averaging phase differences of 10 data sets for AWP data, as given in Fig. 3 *A*. For U = 0, 10, and 15 V_{pp}, the AWP is about constant, i.e., for these driving voltages, no measurable pumping occurred. At higher voltages, the AWP slope over time increased nonlinearly with driving voltage. The curve is a fit of a power function of the driving voltage, U, for voltages above 15 V. For the best fit $U^{2.44}$ was obtained.

For calculation of the actual particle velocity (right axis of Fig. 3 *B*) from the AWPD, identical properties of the particles were assumed. The fringe spacing was calculated from Eq. 1 to be 909 nm for a refractive index of 1.33 and ϑ = 30.35° (see Fig. 1 *A*). Thus 1° rescales to a velocity of 909 nm × 512 Hz/360 = 1.2928 μm/s. The velocity is defined as positive for particle movements in the direction of the TW field.

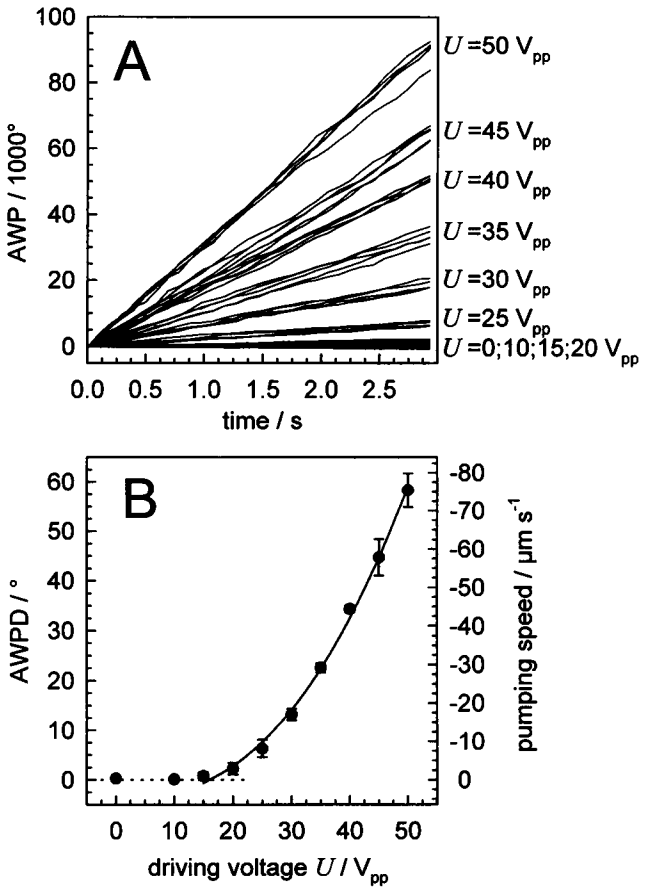

FIGURE 3 PALS measurement of dependence of pumping on the driving voltage U at a TW frequency of 1 MHz and a conductivity of 4 mS/m. The sampling rate was 512 Hz. (*A*) Selected amplitude weighted phases (AWPs). (*B*) Means and standard deviations of amplitude weighted phase differences (AWPDs) of 10 measurements.

Frequency dependence of pumping

For the main peak of TW pumping, the induced liquid streaming and TW field propagation are oppositely directed (Melcher and Firebaugh, 1967; Fuhr et al., 1994). Furthermore, an accumulation of probe particles inside the electrode region has been described (Müller et al., 1993). Because our measuring volume is located outside the electrode structure, two modes are possible, either pumping out of (forward mode) or into (reverse mode) the electrode region. Fig. 4 compares frequency spectra of pumping for the two modes. As can be seen, the spectra are equivalent within the time necessary to detect a complete spectrum. However, to avoid a decrease in particle concentration in the measuring volume due to accumulation of particles within the array, the reverse mode was used for further measurements.

In Fig. 5 the frequency spectra for various solution conductivities up to 16 mS/m are displayed. All spectra exhibit a clear maximum. With increasing conductivity, the frequency of the maximum is shifted toward higher frequencies and the pumping speed strongly increases above 4 mS/m. Conductivities higher than 16 mS/m were not used,

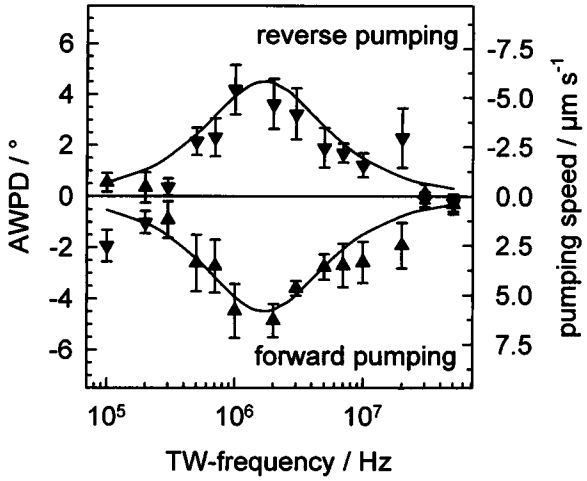

FIGURE 4 Frequency spectra of pumping in forward mode (▲) and reverse mode (▼). The driving voltage was 25 V_{pp}, and the conductivity 4 mS/m. Every point represents 18 measurements. The curves are fits of a single Lorentzian function for the values below 20 MHz.

because of strong thermal convections and electrolytic processes. At 20 MHz, a second maximum was observed. This was especially pronounced for higher conductivities. Its frequency was independent of the conductivity. Further analysis of this phenomenon showed that this additional

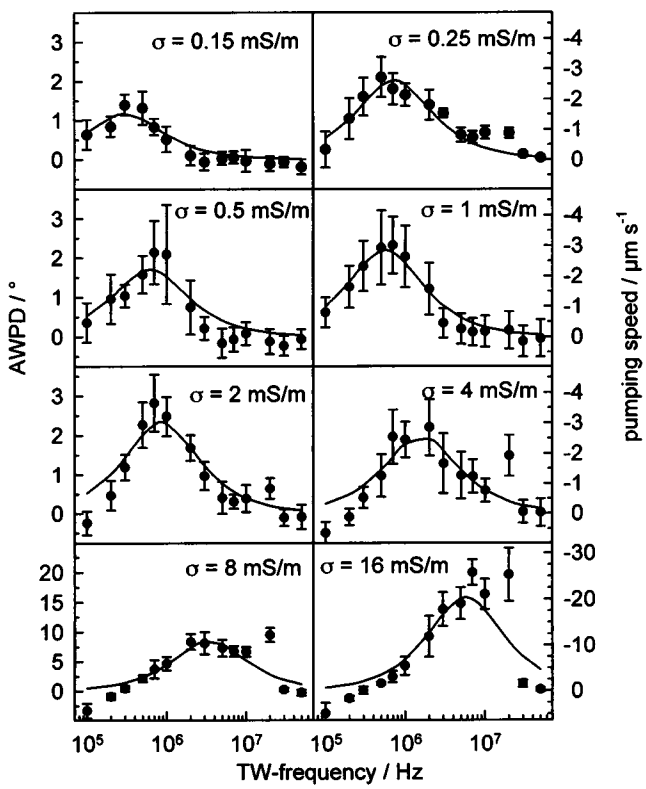

FIGURE 5 Frequency dependence of pumping speed for various conductivities, σ. Each point represents the mean of 10 AWPD spectra. The points around the resonance of 20 MHz were ignored for the fits. The driving voltage was 25 V_{pp}.

maximum was generated by electronic resonance caused by the inherent chamber properties (see below). Müller et al. (1993) showed that pumping up to 2 MHz is due mainly to a single relaxation process that can be described by a single Lorentzian. Therefore, to determine peak frequencies and pumping speeds by fitting, the points around the resonance at 20 MHz were ignored.

Chamber resonance

As can be seen in Fig. 5, the distortion of the Lorentzian behavior around 20 MHz became stronger for higher conductivities. At 8 mS/m it was especially pronounced, and the 20 MHz peak even exceeded the height of the relaxation peak. For analysis, the frequency dependence of pumping around 20 MHz was measured in detail (*circles* in Fig. 6). Obviously the frequency width of the peak is too small to be described by an additional Lorentzian. The high-frequency flank is strongly dampened, and above 30 MHz the pumping effect disappeared. On the lower flank, distortions can be suspected. For all measurements the coaxial cable of the generator was terminated by 50 Ω (Fig. 7). The signal amplitude was checked over these resistors to make sure that it was frequency independent. Therefore, we expected that the resonance was caused by the inductance of the external chamber wiring, in combination with the inherent microchamber properties. The latter properties must be determined by the inductance of the bond wires and the strip electrodes, in combination with the interelectrode capacitances and resistances. To reduce the inductance of the external wiring, we redesigned the external circuitry and located the terminating resistors close to the microchamber. Astoundingly, this measure did not shift the peak.

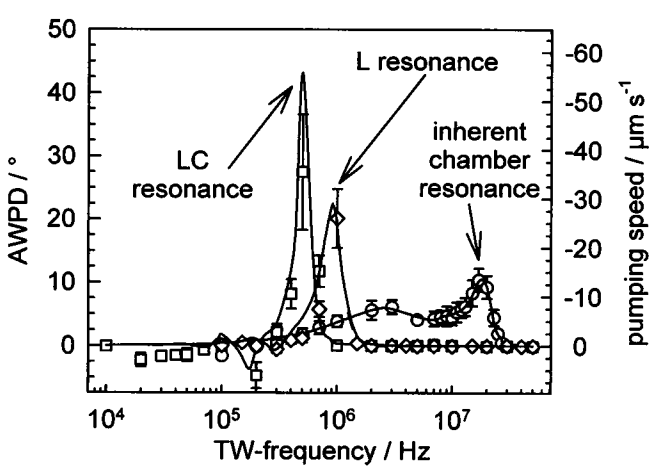

FIGURE 6 Pumping speed as a function of field frequency at a conductivity of 8 mS/m. The micropump was directly connected to the coupling capacitors (○; R_{ch} = 0.4 kΩ), or additional inductances (680 µH, ◇, R_{ch} = 7.5 kΩ) and capacitances (100 pF, □, R_{ch} = 6.7 kΩ) were inserted (compare to Fig. 7, *branches A* and *B*). The curves are fits according to Eqs. A1 and A3, assuming the fitted Lorentzian pump peak of Fig. 5. For electric parameters see text. All fits yielded the same proportionality coefficient of $\mathcal{P}$ = 12 m(Ns)$^{-1}$. Fitted resistances R_{ch} are given above.

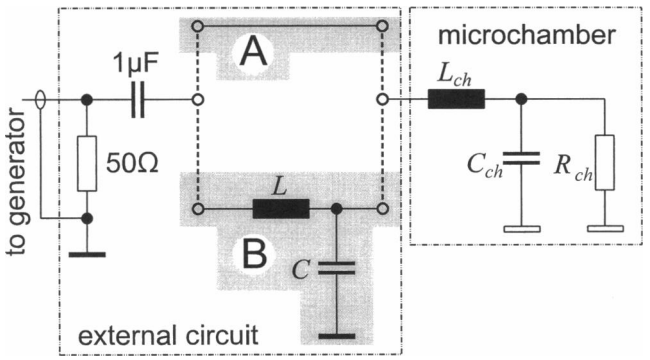

FIGURE 7 Electronic scheme describing the generator load and the TW microchamber properties for one phase of the four driving signals. The signal line was terminated by a 50-Ω resistor and capacitively (C = 1 µF) coupled to the microchamber without additional discrete elements (*branch A*) or through a resonance circuit (*branch B*). C_{ch} and R_{ch}, representing the microchamber properties, are assumed to be at virtual ground.

Only when inductances and capacitances were added as discrete elements (*branch B* of Fig. 7) was the frequency dependence of pumping changed. Only by adding inductances (L = 680 µH) was the resonance peak shifted to 1 MHz at the lower flank of the Lorentzian peak (*diamonds* in Fig. 6). Additional capacitances (C = 100 pF) decreased the resonance frequency to 600 kHz (*squares* in Fig. 6). The peak became more than twice as high as the former 20-MHz peak. In any of these cases, pumping above the resonance was dampened, and a strongly nonmonotonous behavior occurred at the lower flank.

DISCUSSION

In general, depending on their parameters, TW pumps generate nonparabolic streaming profiles, although for our experimental setup deviations are small (Müller et al., 1993). Because our measuring volume is located at a distance of ~1 mm from the driving electrode structure, we suppose a laminar, parabolic streaming profile. Furthermore, the Gaussian light intensity distribution within the measuring volume ensured that a lower weight is assigned to particles in the vicinity of the walls. Thus, when the pumping speed is recalculated from the AWPDs, a mean pumping speed is obtained that is lower than the values of authors working with microscopic observations (Müller et al., 1993; Fuhr et al., 1994).

The conductivity dependence of peak frequencies and pumping peak speeds given in Fig. 5 are summarized in Fig. 8. Both curves of Fig. 8 exhibit a characteristic behavior that has not been described before. Fuhr et al. (1994) assumed a generally linear dependence of conductivity and peak frequency. Our detailed analysis disclosed a more complex behavior. The characteristic location of the calculated peak frequency points relative to the linear regression line (Fig. 8 *B*) was found in all experiments. Moreover, the strong increase in pumping speed for higher conductivities has not

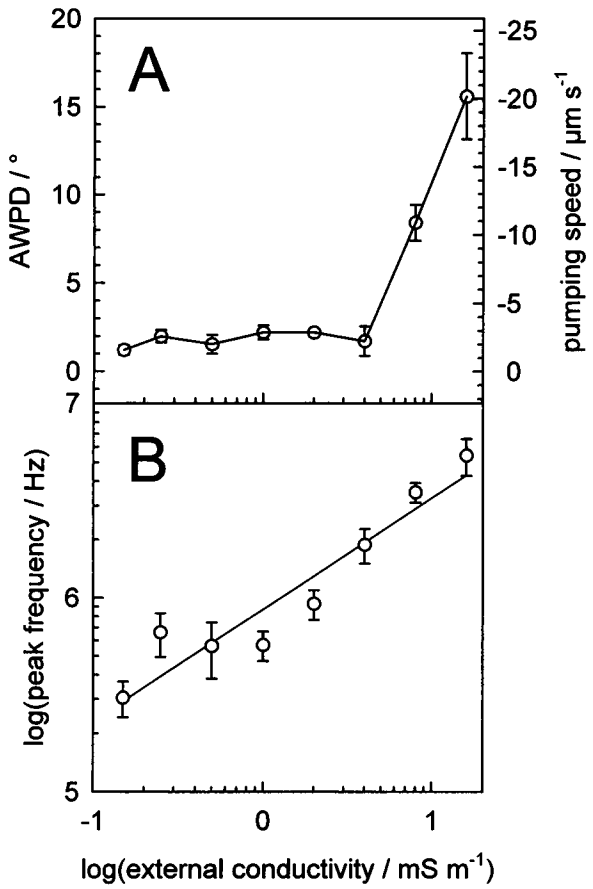

FIGURE 8 Dependence of the Lorentzian pumping peak on the external conductivity. The values were obtained from the fits of Fig. 5. (*A*) Maximum pumping speed. (*B*) Frequency of maximum pumping.

been described before, because previously the conductivity was lower than 16 mS/m.

For conductivities higher than 1 mS/m at the lowest measuring frequencies, pumping in the direction of the TW field was observed (Fig. 5). For lower conductivities this was also found at even lower frequencies (see Fig. 6). This change in the pumping direction was also mentioned by Fuhr et al. (1994) and described by Ehrlich and Melcher (1982). A detailed interpretation is still not available.

When the special properties of the square-topped field and the resonance behavior are neglected, pumping can be described by a single relaxation process, resulting in a Lorentzian frequency behavior (Müller et al., 1993; Fuhr et al., 1994). This suggests that the pumping force evolves from the interaction of induced polarization charges with the external field $\vec{E}$. Usually the polarization is described by $\alpha\vec{E}$, where α is the polarizability. This approach results in an $\vec{E}^2$ dependence of the force. For pumping, a stronger $\vec{E}$ dependence was found (Fig. 3 *B*). Obviously, pumping is influenced by another field strength-dependent process. Most probably, the stronger $\vec{E}$ dependence must be attributed to the generation of a temperature gradient within the measuring solution. This gradient is the prerequisite for the induction of spatial charges necessary for pumping (Müller et al., 1993; Fuhr et al., 1994). Heating in relation to the complex heat dissipation from the pumping system determines the profile of the temperature and therefore of the conductivity and permittivity gradient. It is clear that the gradients, depending on Joule heating, are proportional to the electrical energy dissipated in the system. In Eq. 4 the complex but isotropic process of the thermal generation of a gradient in the dielectric properties of the solution is described by $f_T(\vec{E}_{rms})$:

$$\vec{F}(\omega) \propto f_T(\vec{E}_{rms}) \cdot \alpha\vec{E} \cdot \vec{E} \tag{4}$$

$\vec{F}(\omega)$ is the pumping force. For voltages above 15 V_{pp}, $f_T(\vec{E}_{rms})$ is proportional to $\vec{E}^{\xi}_{rms}$, with ξ close to 0.5:

$$\vec{F}(\omega) \propto \vec{E}^{\xi}_{rms} \cdot \alpha\vec{E}^2 \tag{5}$$

Considerations of the dependence of the pumping speed on the driving voltage yielded a power function with an exponent ranging from 2 to 4 (Fuhr et al., 1994). For our chamber geometry, Müller et al. (1993) predicted 2.5. Our results also show that this dependence is valid for driving voltages above 15 V_{pp}, the lowest voltage used by these authors. From the best fit of our data, an only slightly different value of 2.44 was obtained. This implies that at voltages below 15 V_{pp}, heat dissipation is too low to develop a sufficient temperature gradient for pumping.

It must be expected that for pumping, not only the strength of the induced gradient but also its location are of importance. This is because the quality of the field interacting with the induced spatial charges depends on the distance from the electrode structure. Close to the electrodes, a simple AC character dominates, whereas the TW character will be at maximum only at a certain distance. Then, with increasing distance, the electrode structure can be considered as an equipotential surface. These properties also imply a complex dependence of pumping on chamber geometry, solution, field parameters, and heat dissipation.

How can the resonance increase in pumping speed around 20 MHz be explained? Because the driving voltage at the terminating resistors was frequency independent, the reason for the resonance peak must be located within the chamber structure. Attempts of a direct measurement of the electric chamber properties by a HP4194A impedance analyzer (Hewlett Packard) failed. The impedance of the electrode array exhibited only an extremely low distortion in the phase behavior at the resonance frequency of pumping. Most probably, the array must be described as a cable whose resonance properties at the electrode side cannot simply be detected at the feeding side. From electrorotation measurements it is known that chamber resonance effects can be modeled, assuming the simple circuit of Fig. 7, although the actual chamber properties are poorly reflected (Gimsa et al., 1996). For pumping, this scheme also allowed us to model the measured spectra when the special properties of the square-topped driving field were considered (see Appendix).

All curves of Fig. 6 are fits with consistent parameters of the different electronic parts of Fig. 7. Their values were obtained in the following way. First, the inherent chamber capacitance was determined from the resonance frequency, with only external inductances added. For this it was assumed that the external inductance overwhelmed the inherent chamber inductance. Then the inherent inductance was calculated from the inherent chamber resonance. A capacitance of C_{ch} = 42.5 pF and an inductance of L_{ch} = 1.5 μH were found. Finally, the model was tested by the addition of external capacitances and inductances according to Fig. 7, branch B. After the determination of frequency and height of the pumping peak from the undistorted part of the Lorentzian curve (*circles*), the only remaining parameter was the resistance (R_{ch} in Fig. 7). Obviously, the fitted resistance values given in the legend of Fig. 6 not only reflect the conductivity of the solution, but are also influenced by electronic chamber properties that determine the effective resonance height. These properties are not correctly reflected by our simple model (Fig. 7). For all fits, the same Lorentzian frequency dependence of pumping, the harmonic content of the signals (Eq. A3), and the resonance behavior according to the determined electronic parameters could be assumed. The distortions at the lower frequency flank of the resonance peak could be explained as being caused by higher harmonics already at resonance at lower measuring frequencies. The measured changes in pumping direction due to the resonance of the third harmonics at one-third of the respective resonance peak frequencies are nicely reflected by our theoretical curves. This proves that the non-Lorentzian peak was really caused by electronic resonance.

CONCLUSION

Although the observed pumping behavior can be phenomenologically described, development of a correct theory is an intricate problem and was not the aim of this paper. For this, further experiments on the influence of the pump geometry, electric properties of its housing, the microchip design, and different liquids will be necessary. Our widened conductivity range, in combination with PALS, allowed the identification of a nonlinear dependence of frequency and height of the peak on the external conductivity. The reason for this nonlinear behavior needs to be elucidated.

The widened frequency range allowed examination of the inherent electronic chamber resonance. For characterization of the pumping behavior and of dielectric medium properties above the related cutoff frequency of ~20 MHz, the electronic properties of the microchamber need to be improved. An interesting aspect is that the traveling directions of the harmonics are reflected in the frequency behavior of pumping. This proves in an elegant way that TW pumping is due mainly to field effects, not to isotropic heating effects, a question that was already addressed by balloon experiments under reduced gravity (Müller et al., 1993). For technical applications, integration of capacitances and inductances into the pump device will allow control of pumping efficiency and the use of reduced driving voltages, as already proposed for dielectric micromotors (Müller et al., 1997).

To register inherent particle properties such as conductivities and permittivities, optical microchambers allowing the registration of TW dielectrophoresis above the electrode structure need to be developed. Furthermore, expansion of PALS to dielectrophoretic measurements is under way. These developments will be complementary to ERLS (Gimsa et al., 1995; Prüger et al., 1997) and will help the expansion of laser optical particle characterization to inherent particle properties. We think that the application of PALS to dielectric particle spectroscopy will be a significant breakthrough for dielectric characterization. PALS will overcome the disadvantages of tedious microscopic measurements by computerization as well as statistical significance at short measuring times. In contrast to conventional optical approaches (Talary and Pethig, 1994; Inoue et al., 1988), dynamic light scattering methods allow a direct detection of the frequency dependence of particle motion and avoid particle-particle interactions.

APPENDIX: INFLUENCE OF SQUARE-TOPPED FIELDS AND CHAMBER RESONANCES ON PUMPING

For resistors R_{ch} that are not too small, which reflect the conductive properties of the solution, the microchamber scheme in Fig. 7 exhibits a resonance increase of the voltage U_{ch} over $R_{ch}\|C_{ch}$. U_{ch} increases with increasing frequency before a final drop (see Gimsa et al., 1996):

$$U_{ch} = U \cdot \frac{\sqrt{R_{ch}^2 C_{ch}^2 L_{ch}^2 \omega^4 - 2R_{ch}^2 C_{ch} L_{ch} \omega^2 + L_{ch}^2 \omega^2 + R_{ch}^2}}{R_{ch}} \tag{A1}$$

U is the output voltage of the generator and ω the angular field frequency. The resonance described by Eq. A1 explains the increase in pumping speed at a single frequency, but not the distortions at the lower frequency flank of the resonance peak. To explain the distortions, it must be considered that the electrodes are driven by square-topped signals with a duty cycle of 50%. Every electrode signal ($U(\omega)$) can be developed as a Fourier series:

$$U(\omega) = \frac{4}{\pi} U \,\mathrm{Re}\left[\sum_{n=0}^{\infty} (-1)^n \frac{\exp((-1)^n i(2n+1)\omega t)}{2n+1}\right] \tag{A2}$$

U, t, and i stand for amplitude of the square-topped signal, time, and the imaginary unit, respectively. This series possesses only odd harmonics. To analyze the TW field generated by four such signals of 90°, phase shift voltage, and phase relations of neighboring electrodes must be considered. Analysis shows that the traveling directions of harmonic components change for every component. Their field strengths progressively decrease. These properties were observed in the frequency dependence of pumping (Fig. 6). For modeling in analogy to electrorotation in square-topped fields, only the electrostatic interactions of Fourier components of the same order were considered. The pumping speed $\vec{v}_{pump}(\omega)$ in a square-topped field can then be developed in a series of force components, $\vec{F}(\omega)$, that would arise

in sinusoidal fields (see Gimsa et al., 1988):

$$\vec{v}(\omega) = \mathcal{P} \cdot \vec{F}_{\text{pump}}(\omega) = \mathcal{P} \cdot \left[\vec{F}(\omega) - \frac{\vec{F}(3\omega)}{3^2} + \frac{\vec{F}(5\omega)}{5^2} - + \ldots \right] \quad \text{(A3)}$$

$\mathcal{P}$ is a proportionality factor depending on the pump design, the viscosity of the solution, and the processes responsible for the induction of the spatial charges. In the series, components alternately change their signs and induce forces with negative and positive pumping directions with respect to the propagation direction of the fundamental frequency. Introduction of the resonance behavior of Eq. A1 into Eq. A3 yielded the fits presented in Fig. 6.

Prof. G. Fuhr and Dr. T. Müller are acknowledged for providing the microchamber and for fruitful discussions. We are grateful to Dr. E. Donath for interesting discussions during the early stage of this work. Dr. S. Shirley is acknowledged for help with the manuscript.

This work was supported by Deutsche Forschungsgemeinschaft grants Gi 232/1-1 and Gi 232/1-2.

REFERENCES

Berne, B. J., and R. Pecora. 1976. Dynamic Light Scattering. Wiley, New York.

Ehrlich, R. M., and J. R. Melcher. 1982. Bipolar model for traveling-wave induced nonequilibrium double-layer streaming in insulation liquids. *Phys. Fluids.* 25:1785–1793.

Eppmann, P., J. Gimsa, B. Prüger, and E. Donath. 1996. Dynamic light scattering from oriented, rotating particles: a theoretical study and comparison to electrorotation data. *J. Phys. III (France).* 6:421–432.

Fuhr, G., J. Gimsa, and R. Glaser. 1985. Interpretation of electrorotation of protoplasts. I. Theoretical considerations. *Stud. Biophys.* 108:149–164.

Fuhr, G., R. Hagedorn, T. Müller, W. Benecke, and B. Wagner. 1992. Microfabricated electrohydrodynamic (EHD) pumps for liquids of higher conductivity. *J. Microelectromech. Syst.* 1:141–146.

Fuhr, G., T. Schnelle, and B. Wagner. 1994. Travelling wave-driven microfabricated electrohydrodynamic pumps for liquids. *J. Micromech. Microeng.* 4:217–226.

Gimsa, J., E. Donath, and R. Glaser. 1988. Evaluation of the data of simple cells by electrorotation using square-topped fields. *Bioelectrochem. Bioenerg.* 19:389–396.

Gimsa, J., T. Müller, T. Schnelle, and G. Fuhr. 1996. Dielectric spectroscopy of single human erythrocytes at physiological ionic strength: dispersion of the cytoplasm. *Biophys. J.* 71:495–506.

Gimsa, J., B. Prüger, P. Eppmann, and E. Donath. 1995. Electrorotation of particles measured by dynamic light scattering—a new dielectric spectroscopy technique. *Coll. Surf. A.* 98:243–249.

Hagedorn, R., G. Fuhr, T. Müller, and J. Gimsa. 1992. Travelling-wave dielectrophoresis of microparticles. *Electrophoresis.* 13:49–54.

Inoue, T., R. Pethig, T. A. K. Al-Ameen, J. P. H. Burt, and J. A. R. Price. 1988. Dielectrophoretic behaviour of *Micrococcus lysodikticus* and its protoplast. *J. Electrostat.* 21:215–223.

Jones, T. B. 1995. Electromechanics of Particles. Cambridge University Press, Cambridge, New York, Melbourne.

Kaler, K. V. I. S., O. G. Fritz, and R. J. Adamson. 1988. Dielectrophoretic velocity measurements using quasi-elastic light scattering. *J. Electrostat.* 21:193–204.

Melcher, J. R. 1966. Traveling-wave induced electroconvection. *Phys. Fluids.* 9:1548–1555.

Melcher, J. R., and U. S. Firebaugh. 1967. Traveling wave bulk electroconvection induced across a temperature gradient. *Phys. Fluids.* 10: 1178–1185.

Melcher, J. R., and G. I. Taylor. 1969. Electrohydrodynamics: a review of the role of interfacial shear stresses. *Annu. Rev. Fluid Mech.* 1:111–146.

Miller, J. F., K. Schätzel, and B. Vincent. 1991. The determination of very small electrophoretic mobilities in polar and nonpolar colloidal dispersions using phase analysis light scattering. *J. Colloid Interface Sci.* 143:532–554.

Müller, T., W. M. Arnold, T. Schnelle, R. Hagedorn, G. Fuhr, and U. Zimmermann. 1993. A traveling-wave micropump for aqueous solutions. Comparison of 1g and μg results. *Electrophoresis.* 14:764–772.

Müller, T., J. Gimsa, B. Wagner, and G. Fuhr. 1997. A resonant, dielectric micro-motor driven by low ac-voltages (<6V). *Microsyst. Technol.* 3:163–170.

Paul, R., and M. Otwinowski. 1991. The theory of the frequency response of ellipsoidal biological cells in rotating electrical fields. *J. Theor. Biol.* 148:495–519.

Prüger, B., P. Eppmann, E. Donath, and J. Gimsa. 1997. Measurement of inherent particle properties by dynamic light scattering: introducing electrorotational light scattering. *Biophys. J.* 72:1414–1424.

Sauer, F. A., and R. N. Schlögl. 1985. Torques exerted on cylinders and spheres by external electromagnetic fields: a contribution to the theory of field-induced cell rotation. *In* Interactions between Electromagnetic Fields and Cells. A. Chiabrera, C. Nicolini, and H. P. Schwan, editors. Plenum Publishing, New York. 203–251.

Schätzel, K. 1987. Correlation techniques in dynamic light scattering. *J. Phys. B.* 42:193–213.

Schätzel, K., and J. Merz. 1984. Measurement of small electrophoretic mobilities by light scattering and analysis of the amplitude weighted phase structure function. *J. Chem. Phys.* 81:2482–2488.

Schnelle, T., R. Hagedorn, G. Fuhr, S. Fiedler, and T. Müller. 1993. Three-dimensional electric field traps for manipulation of cells—calculation and experimental verification. *Biochim. Biophys. Acta.* 1157: 127–140.

Talary, M. S., and R. Pethig. 1994. Optical technique for measuring the positive and negative dielectrophoretic behaviour of cells and colloidal suspensions. *IEE Proc. Sci. Meas. Technol.* 141:395–399.

Wang, X.-B., Y. Huang, F. F. Becker, and P. R. C. Gascoyne. 1994. A unified theory of dielectrophoresis and travelling wave dielectrophoresis. *J. Phys. D Appl. Phys.* 27:1571–1574.